EVOLUTION OF EARTHQUAKE HAZARDS IN İZMİR IN RESPONSE TO M4+ EARTHQUAKES

by

Tolunay Yılmaz

B.S., Geomatics Engineering, Karadeniz Technical University, 2018

Submitted to the Kandilli Observatory and Earthquake

Research Institute in partial fulfillment of

the requirements for the degree of

Master of Science

Graduate Program in Geodesy

Boğaziçi University

2022

ACKNOWLEDGEMENTS

First, I could not have undertaken this journey without the great support of my thesis advisor Assoc. Prof. Fatih Bulut. He was not only a thesis advisor to me, but also, he was a life coach, a bigger brother to me. He helped me to overcome all the struggles I encountered during my study. He kindly shared all the knowledge he could give and guided me along this path. I also would like to thank Prof. Aslı Garagon for spending her valuable time to help me complete my thesis.

I would like to extend my sincere thanks to faculty members of the Geodesy Department of the Kandilli Observatory and Earthquake Research Institute, Prof. Haluk Özener, Prof. Semih Ergintav, Asst. Prof. Tülay Kaya Eken, Dr. Onur Yılmaz, Dr. Aslı Sabuncu for their insights and support during lectures. Thanks should also go to my class mates during lectures, they helped me whenever I need them.

Last but not least, I would like to express my sincere gratitude to my mother, father, sister and my furry friend Faruk for being there for me and providing me with emotional support.

ABSTRACT

EVOLUTION OF EARTHQUAKE HAZARDS IN İZMİR IN RESPONSE TO M4+ EARTHQUAKES

In this study, we investigated the evolution of earthquake hazards in İzmir (Turkey), the city accommodating the third highest population in Turkey in response to M4+ size earthquakes analyzing Coulomb stress change on all potential receiver faults in the target region. The city is located in western Turkey, which falls under Aegean tectonics, which leads to very high earthquake activity in the region. Fault segments with increasing Coulomb stress host high earthquake activity verifying that M4+ earthquakes prepone the generation processes of some earthquakes. In contrast, fault segments with decreasing Coulomb stress host earthquake silence verifying that M4+ earthquakes postpone the generation processes of some earthquakes. Hence, M4+ earthquakes played a critical role in the occurrence of the 2021 Samos Earthquake (M 6.92) as they increased the Coulomb stress above 0.1 bars along its rupture plane. To sum up, our results show that Coulomb stress change generated by M4+ earthquakes plays a critical role in earthquake activity in the vicinity of İzmir, Turkey.

ÖZET

İZMİR’DEKİ DEPREM TEHLİKESİNİN M4+ DEPREMLERE İLİŞKİN DEĞİŞİMİ

Bu çalışmada, hedef bölgedeki tüm potansiyel alıcı faylar üzerindeki M4+ büyüklüğündeki depremlerin sebep olduğu Coulomb stres değişimini analiz ederek Türkiye'nin en yüksek üçüncü nüfusunu barındıran İzmir'deki (Türkiye) deprem tehlikesinin gelişimini araştırdık. Şehir, bölgede çok fazla deprem aktivitesine yol açan Ege tektoniğinin içinde Türkiye'nin batısında yer almaktadır. Artan Coulomb stresine sahip fay segmentleri, M4+ depremlerinin bazı depremlerin oluşum süreçlerini önceden oluşturduğunu doğrulayan yüksek deprem aktivitesine ev sahipliği yapmaktadır. Dolayısıyla, M4+ depremleri, kırılma düzlemi boyunca Coulomb stresini 0.1 barın üzerine çıkardıkları için 2021 Sisam Depreminin (M 6.92) meydana gelmesinde rol oynamıştır. Çalışmadan elde edilen bulgular, M4+ depremlerin ürettiği Coulomb stres değişiminin İzmir civarındaki deprem aktivitesinde rol oynadığını göstermektedir.

TABLE OF CONTENTS

LIST OF FIGURES

LIST OF TABLES

LIST OF SYMBOLS

c	Cohesion
D	Dip slip
L	Lateral slip
M	Magnitude
Mw	Moment Magnitude
M_0	Seismic moment (dyne-cm)
RL	Rupture length (km)
RW	Rupture width (km)
S	Average displacement (m)
φ	Angle of friction
θ	Dip angle
σ_n	Normal stress
τ	Shear stress on plane

LIST OF ACRONYMS/ABBREVIATIONS

AFAD	Turkey Disaster and Emergency Management Authority catalogs
AUTH	Aristotle University of Thessaloniki
CFS	Coulomb Failure Stress
cm	Centimeter
ETHZ	Eidgenössische Technische Hochschule Zurich
GFZ	GeoforshungsZentrum
INGV	Instituto Nazionale Di Geofisica E Vulcanologia
km	Kilometer
KOERI	Kandilli Observatory and Earthquake Research Institute
Lat	Latitude
Lon	Longitude
mm	Milimeter
NOA	National Observatory of Athens
UOA	University of Athens
yr	Year

1. INTRODUCTION

An earthquake is an abrupt release of strain energy that has accumulated over the years mainly due to tectonic loading. Although tectonic loading plays a major role, recent studies over the last decades have shown that earthquakes might be triggered if the faults are strained up to the ready-to-fail stage [1]. The triggering occurs by Coulomb stress change, where a nearby earthquake redistributes the stress state on a receiver fault [2]. Here, earthquake-triggering Coulomb stress change refers to an increase in shear stress or a decrease in fault normal stress.

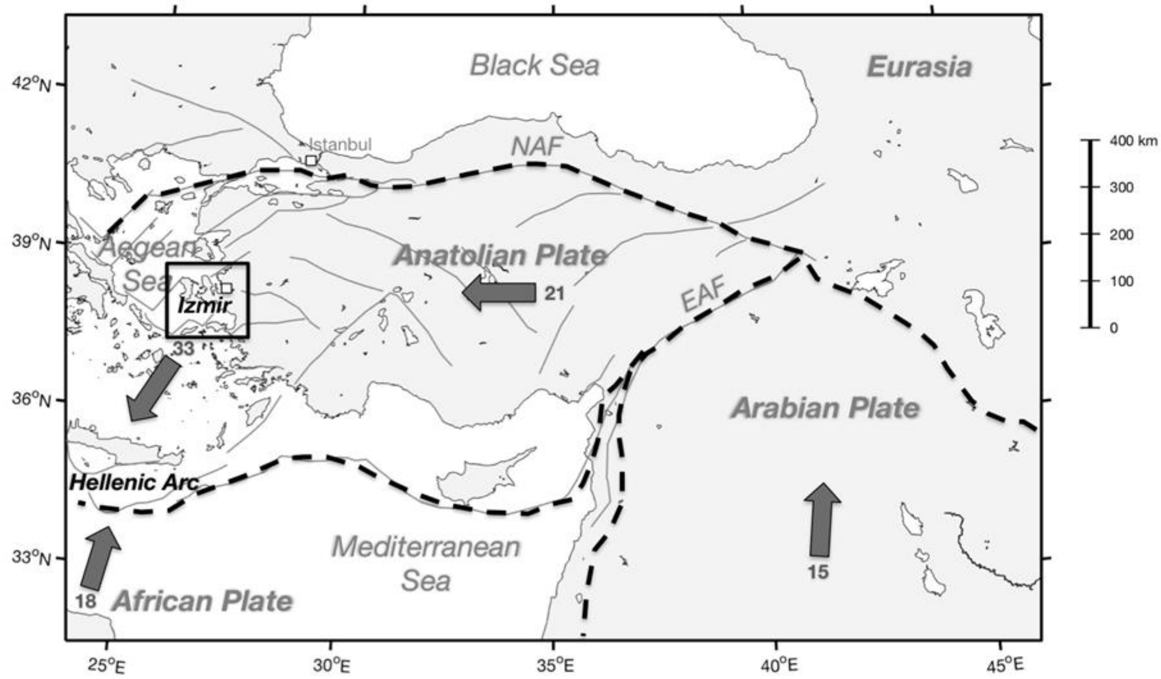

Figure 1.1. Tectonic frame surrounding the target region taken from work of of Reilinger et al., (2006), Bulut et al. (2012) and Yaltırak et al. (2012). Dashed lines show plate boundaries. Gray solid lines show major active faults. Black arrows with numbers represent the magnitude of plate velocities in mm/yr. The study area for this thesis is indicated by a solid black rectangle.

This investigation requires two basic inputs [2]. The first input is the locations and focal mechanisms of the source earthquakes redistributing the stress state in the Earth's crust and therefore changing the Coulomb stress on receiver faults. The second input is the geometry and the kinematics of the receiver faults on which the earthquake hazard increases or decreases in response to source earthquakes. Constructing these two databases would allow us to investigate changes in earthquake hazards, which is especially essential to monitor in the vicinity of highly populated cities.

In this study, we investigated the evolution of earthquake hazards in İzmir (Turkey), the city accommodating the third highest population in Turkey, in response to M4+ size earthquakes. The city is located in western Turkey, which falls under Aegean tectonics, resulting in very high earthquake activity in the region. The extensional features dominate Aegean tectonics [3]. Northward moving African Plate subducting below the Aegean Sea along the Hellenic Arc is presently in a stage of roll back which leads to a large-scale extension surrounding the target region. Additionally, the westward-moving Anatolian Plate due to this extensional regime in the west and the collisional regime in the east generates transform features in the region. As a result, the region accommodates a remarkably high earthquake activity, which threatens the community. Historical records confirm that İzmir has been exposed to destructive earthquakes in the past, and therefore, it is crucial to investigate the earthquake hazards in its near vicinity (e.g., 10.07.1688 M 7.0 İzmir Earthquake resulted in more than 16000 casualties).

As a reference database of receiver faults, we used a fault map generated by Bulut et al., 2021 [4]. The focal mechanism database was compiled mainly from Kandilli Observatory and Earthquake Research Institute (KOERI), and Turkey Disaster and Emergency Management Authority catalogs (AFAD). Additionally, we used focal mechanisms from Aristotle University of Thessaloniki (AUTH), Eidgenössische Technische Hochschule Zurich (ETHZ), GeoforshungsZentrum (GFZ), Instituto Nazionale Di Geofisica E Vulcanologia (INGV), National Observatory of Athens (NOA), University of Athens (UOA) for the events that are not reported in KOERI or AFAD catalogs. Coulomb stress change on receiver faults was calculated at different focal depths using Coulomb software, which has been developed by Toda et al., 2011 [5]. The results were interpreted to represent the current state of the earthquake hazards in this highly populated region.

2. DATA ANALYSIS

For Coulomb stress change analysis, source earthquakes and receiver faults are basic inputs [2]. To be more precise, source earthquakes must be represented by their locations, rupture planes, focal mechanisms (strike, dip, and rake angles), and average slips. On the other hand, receiver faults must be represented by their locations and kinematics (strike, dip, and rake angles).

2.1. Source Faults

Source earthquakes were compiled from different catalogs. Mainly, they were compiled from the focal mechanism catalogs of Kandilli Observatory and Earthquake Research Institute, and Turkey Disaster and Emergency Management Authority. Additional data were obtained from Aristotle University of Thessaloniki (AUTH), Eidgenössische Technische Hochschule Zurich (ETHZ), GeoforshungsZentrum (GFZ), Instituto Nazionale Di Geofisica E Vulcanologia (INGV), National Observatory of Athens (NOA), University of Athens (UOA) in case the earthquakes were not reported by Kandilli Observatory and Earthquake Research Institute, and Turkey Disaster and Emergency Management Authority.

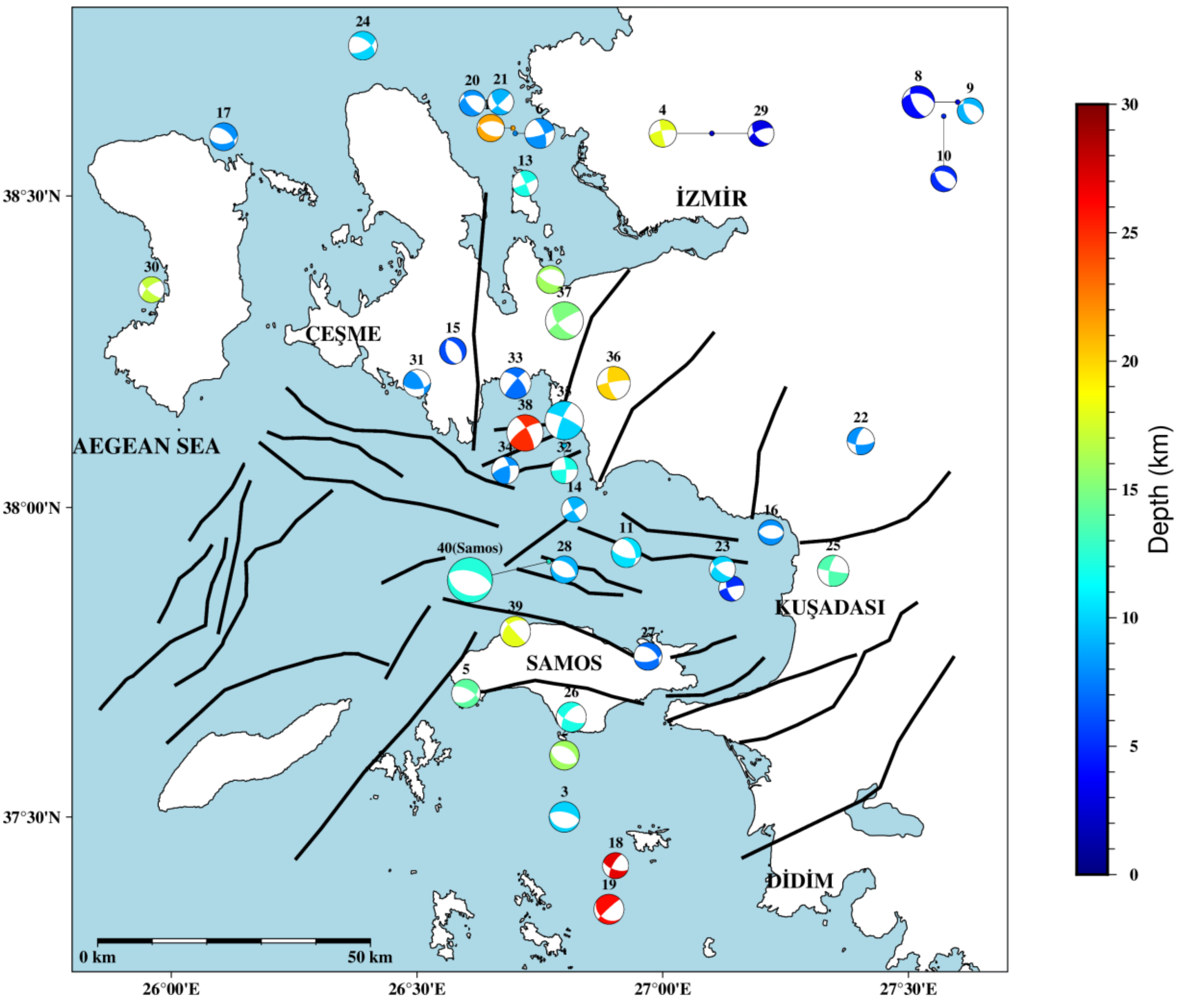

Figure 2.1. Focal mechanisms of M4+ earthquakes are shown within the time period of 2005-2020 in the vicinity of İzmir Region. Black solid lines indicate the active faults generated by Bulut et al., 2021 [4]. Beachballs are color encoded by the event depths.

Table 2.1. Focal mechanisms of analyzed earthquakes obtained from AUTH, UOA, NOA, GFZ, INGV, KOERI, AFAD, Bulut et al., 2021

Event	Year	Month	Day	Institution	Lon. ºE	Lat. ºN	Depth (km)	Strike (°)	Dip (°)	Rake (°)	Magnitude (Mw)
1	2020	7	16	NOA	26.77	38.37	16.00	265	27	-118	4.3
2	2019	8	30	UOA	26.80	37.60	16.00	302	46	-84	4.5
3	2019	8	30	NOA	26.80	37.50	10.00	103	27	-89	4.7
4	2019	1	25	KOERI	27.10	38.60	18.00	259	72	-175	4.2
5	2018	7	26	KOERI	26.60	37.70	14.00	298	64	-52	4.4
6	2017	12	25	KOERI	26.70	38.60	8.00	339	66	-12	4.6
7	2017	5	8	AFAD	27.14	37.87	5.08	160	62	-13	3.9
8	2017	4	21	KOERI	27.60	38.65	4.00	276	45	-138	5
9	2017	4	19	AFAD	27.63	38.64	9.00	288	47	-127	4
10	2017	4	2	AFAD	27.57	38.63	5.00	288	42	-114	4
11	2016	10	17	AFAD	26.93	37.93	10.36	338	43	-44	4.6
12	2016	6	5	AFAD	26.70	38.61	21.34	264	48	-117	4.2
13	2016	4	6	AUTH	26.72	38.52	12.00	336	87	-4	4
14	2015	10	23	KOERI	26.82	38.00	9.00	58	90	173	3.9
15	2015	7	6	KOERI	26.57	38.25	6.00	163	46	-76	4.1

Table 2.1. Focal mechanisms of analyzed earthquakes obtained from AUTH, UOA, NOA, GFZ, INGV, KOERI, AFAD, Bulut et al., 2021 (cont.)

Event	Year	Month	Day	Institution	Lon. ºE	Lat. ºN	Depth	Strike (°)	Dip (°)	Rake (°)	Magnitude (Mw)
16	2015	3	27	KOERI	27.22	37.96	8.00	97	48	-84	3.9
17	2014	12	4	KOERI	26.11	38.59	8.00	310	54	-58	4.3
18	2013	7	25	NOA	26.90	37.42	27.00	109	64	-21	4
19	2013	2	21	AFAD	26.89	37.35	25.98	227	84	-120	4.6
20	2012	5	3	NOA	26.61	38.65	8.00	261	39	-143	4
21	2012	5	2	NOA	26.67	38.65	9.00	47	87	151	4
22	2012	2	20	KOERI	27.40	38.11	8.00	91	67	-29	4.2
23	2011	12	27	KOERI	27.12	37.90	10.00	130	68	-46	4
24	2011	12	5	GFZ	26.39	38.74	10.00	60	61	-138	4.4
25	2010	11	11	KOERI	27.35	37.90	13.60	100	86	-21	4.8
26	2009	6	20	KOERI	26.81	37.66	12.00	112	66	-35	4.6
27	2008	4	11	AUTH	26.97	37.76	7.00	79	58	-124	4.3
28	2008	3	1	AUTH	26.80	37.90	9.00	306	47	-78	4.2
29	2008	1	5	AUTH	27.10	38.60	3.00	247	67	-142	4
30	2007	12	31	NOA	25.96	38.35	17.00	131	72	-26	4

Table 2.1. Focal mechanisms of analyzed earthquakes obtained from AUTH, UOA, NOA, GFZ, INGV, KOERI, AFAD, Bulut et al., 2021 (cont.)

Event	Year	Month	Day	Institution	Lon. ºE	Lat. ºN	Depth (km)	Strike (°)	Dip (°)	Rake (°)	Magnitude (Mw)
31	2006	4	13	KOERI	26.50	38.20	8.00	332	60	138	4.2
32	2005	11	16	NOA	26.80	38.10	12.00	357	80	4	4.1
33	2005	10	31	AUTH	26.70	38.20	7.00	221	82	152	4.8
34	2005	10	29	NOA	26.70	38.10	8.00	352	64	23	4.2
35	2005	10	20	AUTH	26.80	38.10	10.00	295	80	12	5.9
36	2005	10	17	INGV	26.90	38.20	20.00	166	65	-8	5.1
37	2005	10	17	INGV	26.80	38.30	15.00	142	60	-10	5.8
38	2005	10	17	ETHZ	26.70	38.10	25.00	236	72	164	5.6
39	2005	6	23	ETHZ	26.70	37.80	18.00	232	37	-175	4.7

We used only M4+ earthquakes to focus on significant stress changes. Earthquake magnitudes were used to estimate the sizes of rupture planes as well as average slips following the empirical equations developed by Ellsworth, 2003 [6]. For the time period of 2005-2020, we extracted a total 39 earthquakes above magnitude 4 (Table 2.1.). Most of them have normal-type mechanisms as expected from the extensional regime, which is predominant in the region. There are also very few strike-slip mechanisms (Figure 2.1.). They are located mostly in the eastern and northern sections of our target region.

2.2. Receiver Faults

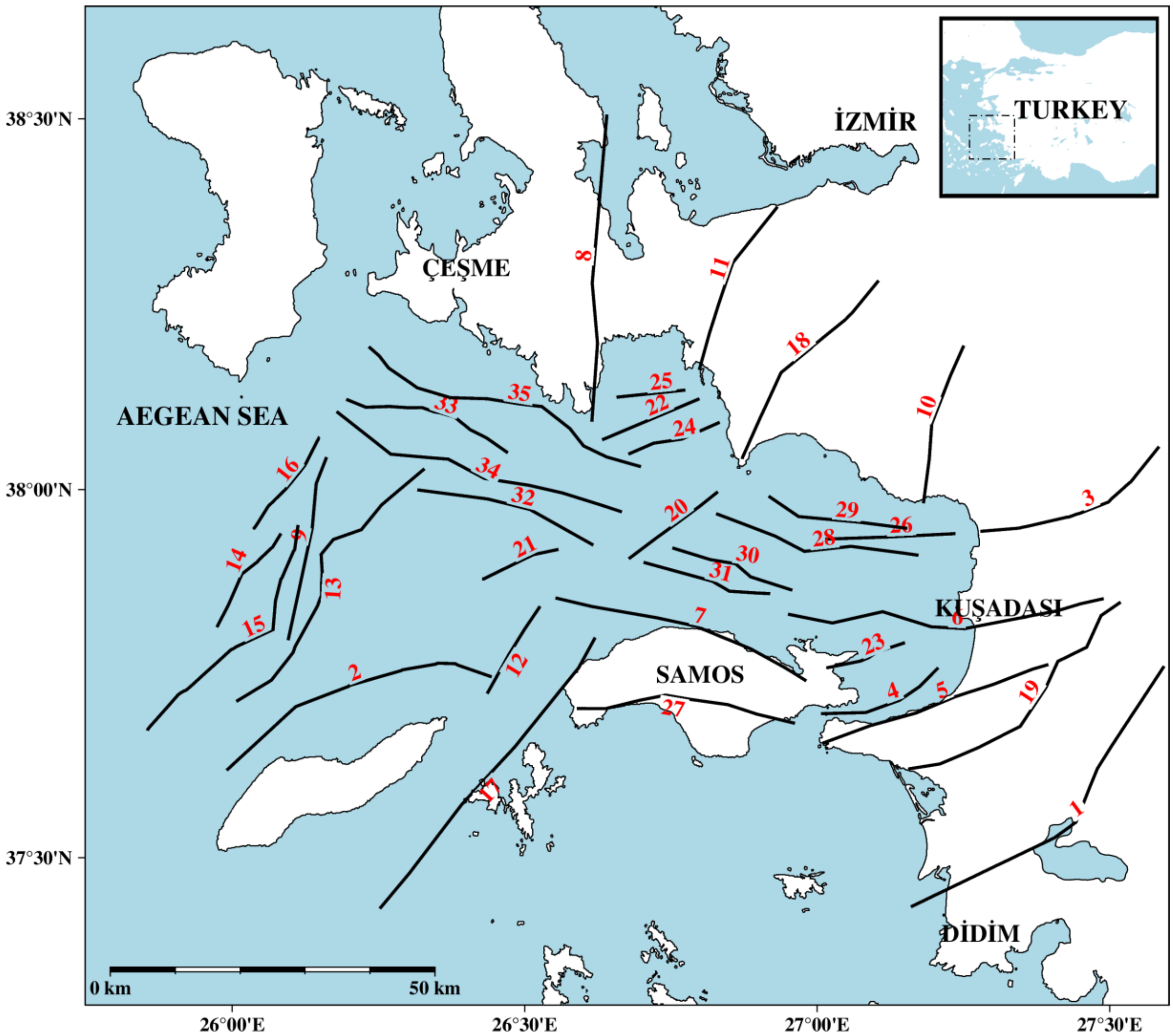

Figure 2.2. Fault map of the study area. Inset map shows the study area in regional scale. Black solid lines with assigned labels show investigated faults which are obtained from Bulut et al., 2021.

We adopted the fault map generated by Bulut et al., 2021 [4], where seismically active faults have been investigated by combining seismic profiles, multi-beam bathymetry, and seismicity. The fault map is shown in Figure 2.2. We investigated a total of 35 receiver faults. Their lengths range from 10 to 55 km. They are predominantly extensional types whereas there are also a few transform types. In Table 2.2, the strike, dip, and rake angles of the receiver faults are given, along with the length of the faults and the Coulomb stress change (ΔCFS) at depths of 8, 10, 12, and 14 kilometers.

Table 2.2. The receiver faults: Their parameters and the CFS changes they accommodate at different depths

Fault ID	Strike (°)	Dip (°)	Rake (°)	Length (km)	ΔCFS 8km (bar)	ΔCFS 10km (bar)	ΔCFS 12km (bar)	ΔCFS 14km (bar)
1	50	65	270	55	-0.011	-0.006	-0.004	-0.005
2	50	70	270	45	0.003	0.003	0.002	0.003
3	55	55	270	31	-0.025	-0.013	-0.097	0.018
4	65	70	270	20	-0.036	-0.016	-0.014	-0.012
5	71	70	270	36	-0.030	-0.013	-0.012	-0.010
6	80	60	270	49	-0.064	-0.023	0.233	-0.020
7	100	70	270	40	0.240	0.101	0.074	0.040
8	180	90	200	45	0.207	0.144	0.098	0.112
9	191	85	200	25	0.020	0.009	0.007	0.006
10	196	90	200	25	0.062	0.032	0.042	0.047
11	205	90	200	27	-0.471	-0.477	-1.871	-0.131
12	210	85	200	15	-0.011	-0.004	0.008	0.003
13	215	80	200	48	-0.006	-0.003	-0.004	-0.002
14	215	80	200	17	-0.005	-0.002	-0.003	-0.002
15	215	80	200	41	-0.006	-0.003	-0.002	-0.002
16	215	80	201	17	0.001	0.001	-0.002	-0.001
17	215	90	200	52	0.009	0.005	0.003	0.003
18	220	85	200	34	-6.326	-5.654	-1.350	0.719
19	230	65	270	44	-0.012	0.014	-0.010	-0.008
20	235	85	200	16	0.700	0.496	0.182	-0.161
21	240	85	200	12	0.012	0.010	0.017	0.006

Table 2.2. The receiver faults: Their parameters and the CFS changes they accommodate at different depths (cont.).

Fault ID	Strike (°)	Dip (°)	Rake (°)	Length (km)	ΔCFS 8km (bar)	ΔCFS 10km (bar)	ΔCFS 12km (bar)	ΔCFS 14km (bar)
22	245	60	270	16	0.413	-0.766	-0.981	-0.207
23	245	70	270	12	-0.021	-0.017	-0.013	-0.009
24	245	60	270	15	0.811	0.115	1.538	-0.335
25	265	60	270	10	0.913	-0.369	-0.462	0.139
26	265	70	270	20	-0.012	-0.006	0.004	0.005
27	270	65	270	34	0.034	0.030	0.105	0.028
28	280	70	270	32	-0.057	0.013	0.076	-0.008
29	285	60	270	22	-0.031	0.188	0.065	-0.012
30	285	60	270	19	0.085	0.057	0.084	0.018
31	285	60	270	20	0.046	0.039	0.038	0.012
32	285	70	270	28	0.055	0.089	0.155	0.026
33	285	80	270	27	-0.009	-0.005	-0.017	0.005
34	290	80	270	47	0.312	0.179	0.076	-0.017
35	290	80	270	47	0.766	0.242	-0.125	0.034

2.3. Coulomb Stress Change

To investigate Coulomb stress changes, we used Coulomb software developed by Toda et al., 1994 [5]. The software basically calculates fault-normal and shear stress changes on receiver faults in response to source earthquakes using Okada’s elastic equations to calculate point-to-point elastic changes from every patch on ruptured planes of source earthquakes to every patch on receiver faults based on their kinematics [7].

Coulomb’s criterion is still one of the most valid criteria for explaining rock failure [2]. They hypothesized that rock failure occurs under compression when the shear stress, subparallel to a particular plane, exceeds rock's inherent cohesiveness as well as the frictional force resisting against the slide along the failure plane [8].

$$\tau = c + \sigma_n tan\varphi \tag{1}$$

where σ_n is the normal stress acting on the fault plane, c is the cohesion of the material and φ is the angle of friction. Since the sign of τ indicates only the direction, instead of writing Eq (1) as $|\tau|$, the absolute value of sign can be eliminated for simplicity [8].

The ratio of the vertical to horizontal stresses determines whether the source mechanism becomes strike-slip or dip-slip while in the two-dimensional case, only the direction of the regional stress matters. Alternative approaches must be used since direct information on relative stress amplitudes is not frequently available and changes with depth. One approach is to choose the relative stresses that the computations can converge the actual earthquake processes. Another one is to proactively identify the Coulomb changes on all potential fault orientations. These two options are distinct in theory, but in practice, they are not, because focal mechanisms are the best indicators of relative stresses and fault orientations. The distributions of Coulomb stress changes for dip-slip and strike-slip faulting are similar when the two primary stresses are approximately equal.

2.4. Rupture Length and Displacement

There are several empirical relationships that have been developed to estimate rupture length, width, and slip based on the magnitude of an earthquake. These relationships are based on observations of past earthquakes and can provide a rough estimate of these parameters based on the magnitude of the earthquake. However, it is important to note that these relationships are approximate and may not always give accurate results, particularly for earthquakes that differ significantly from the ones used to develop the relationships.

One commonly used relationship for estimating rupture length is the Wells and Coppersmith model [9], which relates rupture length to magnitude using the following equation:

$$M_w = \frac{2}{3} * \log(M_0) - 10.7 \tag{2}$$

where M_w is the moment magnitude, M_0 is the seismic moment of the earthquake, which is a measure of the amount of energy released.

$$S = \sqrt{\frac{M_0}{3.4} * 10^9} \tag{3}$$

where S is the average slip on a fault during an earthquake based on the seismic moment of the earthquake.

$$D = S * \sin(\theta) \tag{4}$$

$$L = S * \cos(\theta) \tag{5}$$

where D is the dip slip, L is the lateral slip, S is the average slip, and θ is the dip angle.

$$A = M_0 / \left(\frac{S}{1000} * 10^{19}\right) \tag{6}$$

where A is the rupture area of an earthquake based on the seismic moment M_0 and the average slip S on the fault.

It is possible to estimate the length and width of an earthquake based on the rupture area of the earthquake, but the relationship between the rupture area and the length and width is not necessarily straightforward.

$$RL = A * 0.4 \tag{7}$$

$$RW = A/RL \tag{8}$$

where RL is the rupture length, RW is the rupture width of an earthquake based on the rupture area of the earthquake.

It is worth noting that this formula is based on the assumption that the seismic moment is proportional to the product of the rupture area, the average slip on the fault, and the shear stress drop across the fault. The accuracy of the estimate of the rupture area will depend on the validity of this assumption, as well as the quality and resolution of the available data.

3. RESULTS

A total of 39 earthquakes were analyzed to calculate the Coulomb stress change generated on 35 receiver faults. Earthquake magnitudes were used to estimate the rupture sizes and average slips of source earthquakes. Their rupture sizes range from 0.79 to 13.19 km. On the other hand, their average slips range from -14cm to 24cm. These estimates are provided in Table 3.1.

Table 3.1 Estimated rupture lengths, rupture widths and slips of the earthquakes analyzed in this study.

Event ID	Year	Month	Day	RL (km)	RW (km)	L (cm)	D (cm)
1	2020	7	16	1.38	1.24	-1.38	-0.73
2	2019	8	30	1.83	1.50	-2.19	0.23
3	2019	8	30	2.43	1.81	-3.11	0.05
4	2019	1	25	1.20	1.13	-0.11	-1.31
5	2018	7	26	1.59	1.36	-1.46	1.14
6	2017	12	25	2.11	1.65	-0.55	2.56
7	2017	5	8	0.79	0.85	-0.18	0.76
8	2017	4	21	3.71	2.40	-3.50	-3.89
9	2017	4	19	0.91	0.94	-0.74	-0.56
10	2017	4	2	0.91	0.94	-0.85	-0.38
11	2016	10	17	2.11	1.65	-1.82	1.89
12	2016	6	5	1.20	1.13	-1.17	-0.60
13	2016	4	6	0.91	0.94	-0.06	0.93
14	2015	10	23	0.79	0.85	0.10	-0.78
15	2015	7	6	1.04	1.03	-1.07	0.27
16	2015	3	27	0.79	0.85	-0.78	0.08
17	2014	12	4	1.38	1.24	-1.32	0.83
18	2013	7	25	0.91	0.94	-0.33	0.87
19	2013	2	21	2.11	1.65	-2.27	-1.31
20	2012	5	3	0.91	0.94	-0.56	-0.74
21	2012	5	2	0.91	0.94	0.45	-0.81
22	2012	2	20	1.20	1.13	-0.64	1.15
23	2011	12	27	0.91	0.94	-0.67	0.65
24	2011	12	5	1.59	1.36	-1.24	-1.38
25	2010	11	11	2.80	1.99	-1.33	3.46
26	2009	6	20	2.11	1.65	-1.50	2.15
27	2008	4	11	1.38	1.24	-1.29	-0.87
28	2008	3	1	1.20	1.13	-1.29	0.27
29	2008	1	5	0.91	0.94	-0.57	-0.73
30	2007	12	31	0.91	0.94	-0.41	0.84

Table 3.1 Estimated rupture lengths, rupture widths and slips of the earthquakes analyzed in this study (cont.).

Event ID	Year	Month	Day	RL (km)	RW (km)	L (cm)	D (cm)
31	2006	4	13	1.20	1.13	0.88	-0.98
32	2005	11	16	1.04	1.03	0.08	1.10
33	2005	10	31	2.80	1.99	1.74	-3.27
34	2005	10	29	1.20	1.13	0.51	1.21
35	2005	10	20	13.19	5.58	5.15	24.21
36	2005	10	17	4.27	2.63	-0.87	6.16
37	2005	10	17	11.46	5.08	-3.62	20.51
38	2005	10	17	8.64	4.21	4.06	-14.17
39	2005	6	23	2.43	1.81	-0.27	-3.10

Coulomb stress changes on receiver faults were calculated for different focal depths (8, 10, 12, and 14 km) in order to investigate the depth variation of earthquake triggering potential. The results show that decreases and increases in Coulomb stress are evenly distributed on average. Coulomb stress decreases reach down to -6.326 bars. Coulomb stress increases reach up to 1.54 bars.

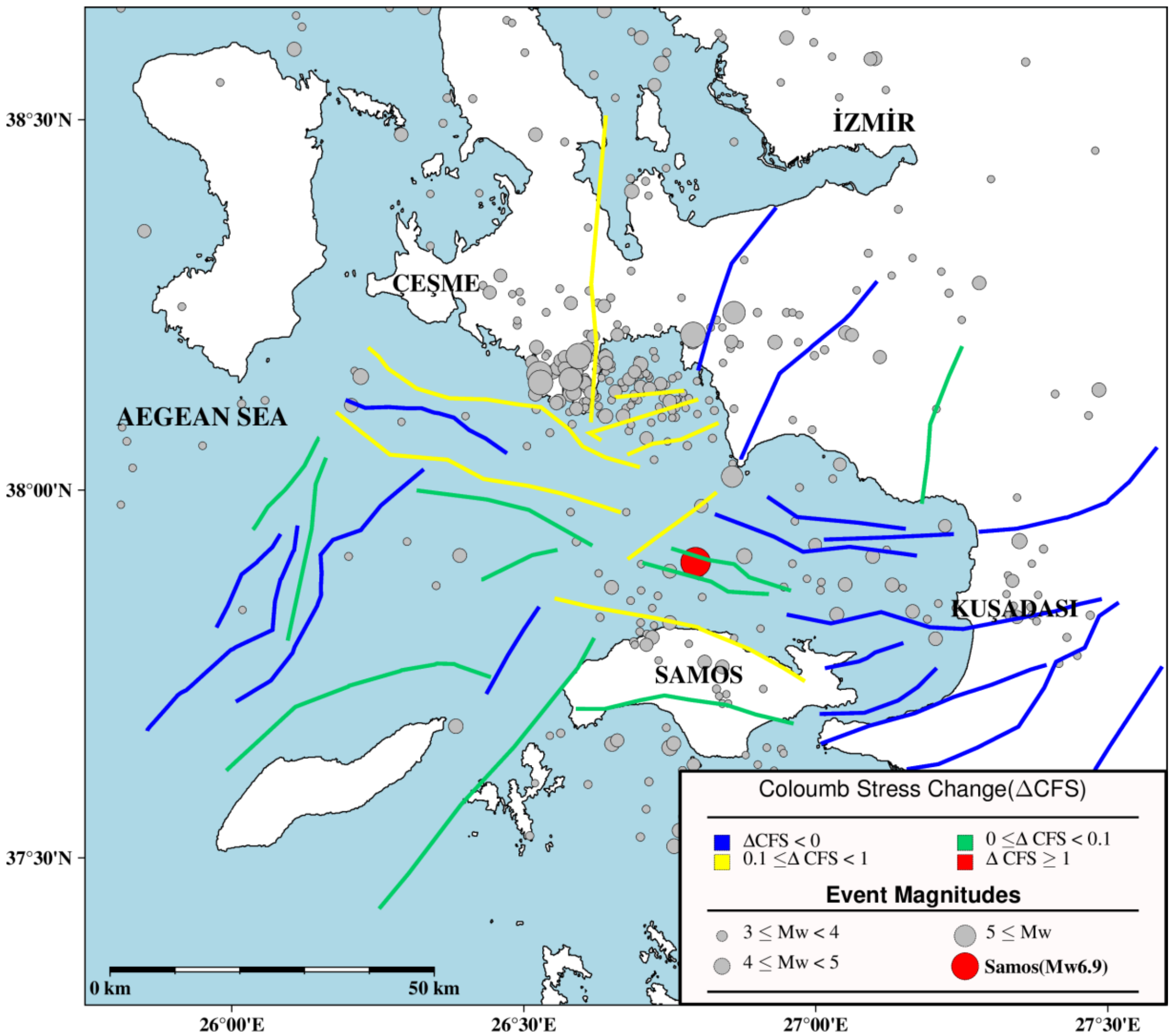

Figure 3.1. Solid lines show the receiver faults. They are color-encoded solid with respect to the coulomb stress change over the faults at 8 km depth. Red dot shows the epicenter of the 2020 Samos earthquake. Gray filled circles show the seismicity around the region between 2005 and 2020.

At 8 km depth, seventeen fault segments accommodate a decrease in Coulomb stress ranging from -6.33 to 0.00 bars. Ten fault segments accommodate an increase in Coulomb stress ranging from 0 to 0.1 bars. Eight fault segments accommodate an increase in Coulomb stress ranging from 0.1 to 1.0 bars. At this depth, there are no fault segments that accommodate an increase above 1.0 bars (Figure 3.1.).

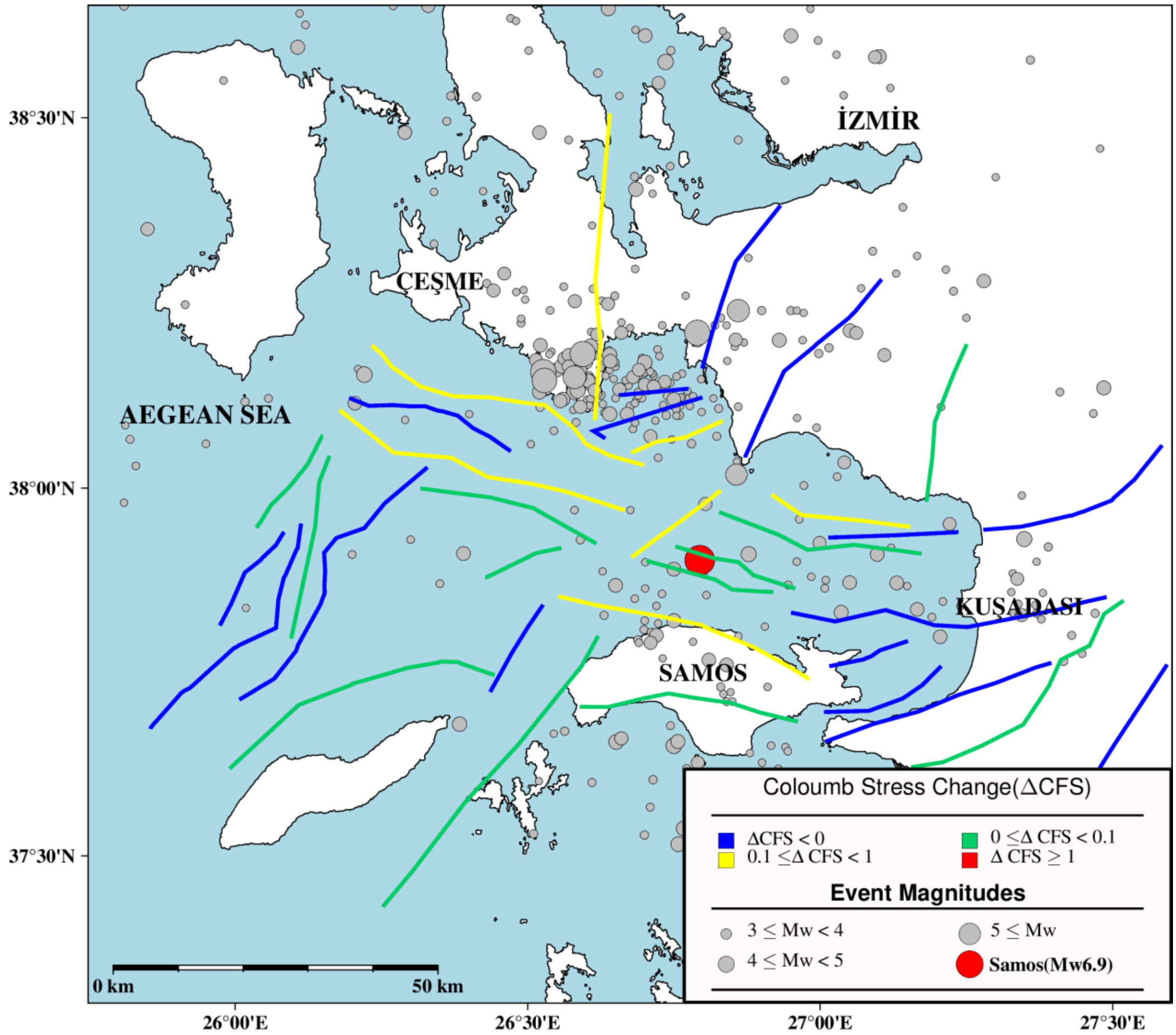

Figure 3.2. Solid lines show the receiver faults. They are color-encoded solid with respect to the coulomb stress change over the faults at 10 km depth. Red dot shows the epicenter of the 2020 Samos earthquake. Gray filled circles show the seismicity around the region between 2005 and 2020.

At 10 km depth, sixteen fault segments accommodate a decrease in Coulomb stress ranging from -5.65 to 0 bars. Twelve fault segments accommodate an increase in Coulomb stress ranging from 0 to 0.1 bars. Seven fault segments accommodate an increase in Coulomb stress ranging from 0.1 to 1.0 bars. At this depth, there are no fault segments that accommodate an increase above 1.0 bars (Figure 3.2).

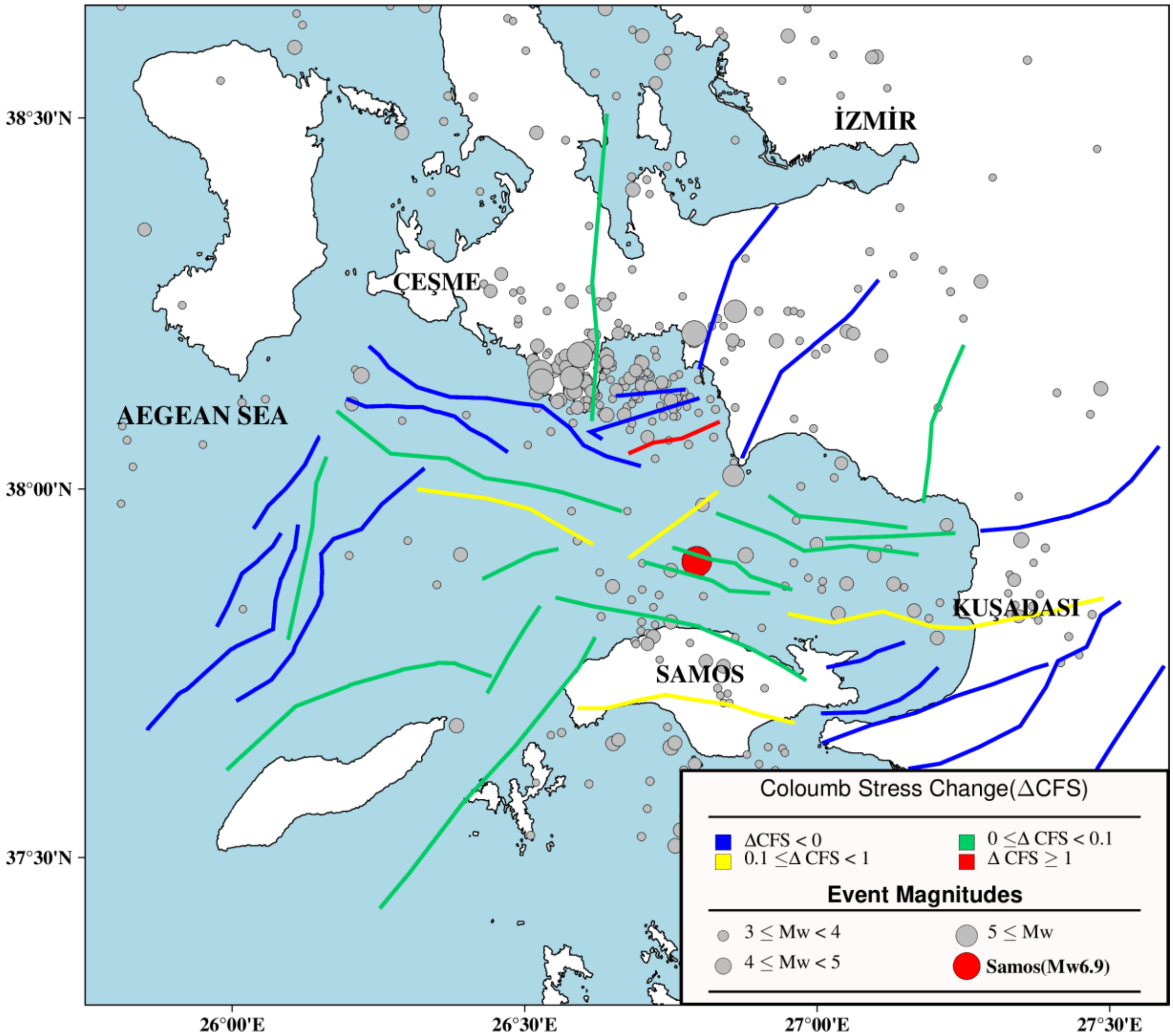

Figure 3.3. Solid lines show the receiver faults. They are color-encoded solid with respect to the coulomb stress change over the faults at 12 km depth. Red dot shows the epicenter of the 2020 Samos earthquake. Gray filled circles show the seismicity around the region between 2005 and 2020.

At 12 km depth, sixteen fault segments accommodate a decrease in Coulomb stress ranging from -1.87 to 0 bars. Fourteen fault segments accommodate an increase in Coulomb stress ranging from 0 to 0.1 bars. Four fault segments accommodate an increase in Coulomb stress ranging from 0.1 to 1.0 bars. At this depth, there is only one fault segment that accommodates an increase above 1.0 bars (Figure 3.3.). This segment has a length of 15 km and therefore has the potential to generate an earthquake in a magnitude range of M5 to M6.

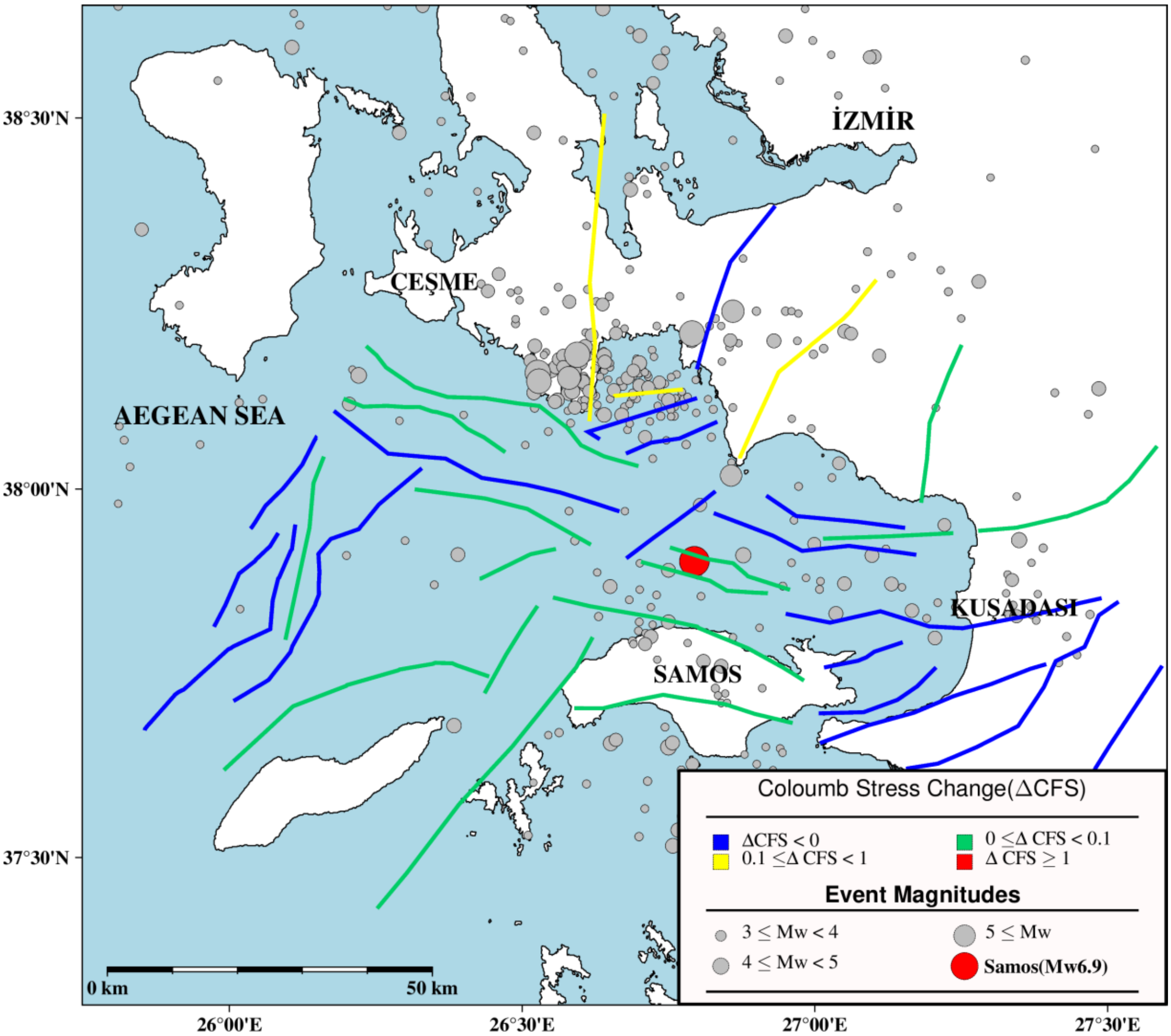

Figure 3.4. Solid lines show the receiver faults. They are color-encoded solid with respect to the coulomb stress change over the faults at 14 km depth. Red dot shows the epicenter of the 2020 Samos earthquake. Gray filled circles show the seismicity around the region between 2005 and 2020.

At 14 km depth, seventeen fault segments accommodate a decrease in Coulomb stress ranging from -0.33 to 0 bars. Fifteen fault segments accommodate an increase in Coulomb stress ranging from 0 to 0.1 bars. Three fault segments accommodate an increase in Coulomb stress ranging from 0.1 to 1.0 bars. At this depth, there are no fault segments that accommodates an increase above 1.0 bars (Figure 3.4.).

4. DISCUSSION

In principle, Coulomb stress increase should prepone failure of receiver faults and therefore trigger earthquakes. This theorem might be tested by comparing the fault segments where the Coulomb stress increases and the following earthquake activity. Our results show that earthquake activity is mostly concentrated along the fault segments where the Coulomb stress increases above 0.1 bars. This is consistent with the triggering threshold [10]. They have previously shown that the triggering might occur if the Coulomb stress increase is larger than 0.1 bars.

On the contrary, Coulomb stress decrease should postpone the failure of receiver faults. This idea might be tested by comparing the fault segments where the Coulomb stress decreases and the earthquake activity they host. Our results show that the fault segments with Coulomb stress decreases are almost silent, accommodating no activity. In this frame, Coulomb stress change plays a critical role in the earthquake generation process in the region postponing or preponing the earthquakes.

An M 6.92 earthquake shook the region on October 30, 2021. This earthquake occurred on the northern shore of Samos Island [4]. In this study, we included this fault segment in our calculations. Our results show that Coulomb stress has increased along this segment. At 12, and 14 km depths, Coulomb stress increase remains below 0.1 bars. However, at 8 and 10 km depths, this increase is above 0.1 bars, which is beyond the triggering threshold [10]. This shows that the M4+ earthquake in the region for the time period of 2005-2020 played a role in the generation of the 2021 Samos Earthquake (M 6.92).

An earthquake is an elastic rebound of the Earth's crust elastically deforming over the years due to a steady-state tectonic loading [11]. Specifically in this target region, GPS measurements have verified that some of the fault segments investigated in this study are routinely strained by the tectonic loading [12]. Our observations verify that the Coulomb stress change has a significant influence on the failure of fault segments at a ready-to-fail stage, in addition to the tectonic strain accumulation.

5. CONCLUSIONS

1. Fault segments with Coulomb stress increase accommodate high earthquake activity verifying that M4+ earthquakes accelerated the generation processes of some earthquakes.

2. In contrast, fault segments with Coulomb stress decrease accommodate earthquake silence verifying that M4+ earthquakes decelerated generation processes of some earthquakes.

3. Specifically, M4+ earthquakes played a role in the occurrence of the 2021 Samos Earthquake (M 6.92) as they increased the Coulomb stress above 0.1 bars along its rupture plane.

4. We have identified a 15 km long fault segment with a Coulomb stress increase of 1.54 bars. This segment is located at a 40 km distance to İzmir in the southwest and has the potential to generate up to M 6 earthquake.

5. In summary, our results show that Coulomb stress change generated by M4+ earthquakes play a role in earthquake activity in the vicinity of İzmir, Turkey.

REFERENCES

1. Stein, R. S., A. A. Barska and J. H. Dieterich, "Progressive Failure on the North Anatolian Fault since 1939 by Earthquake Stress Triggering", *Geophysical Journal International*, Vol. 128, No. 3, pp. 594–604, 1997.

2. King, G. C., R. S. Stein and J. Lin, "Static Stress Changes and the Triggering of Earthquakes.", *Bulletin of the Seismological Society of America*, 84(3), 935-953, 1994.

3. Jackson, J. and D. McKenzie, "Rates of Active Deformation in the Aegean Sea and Surrounding Regions.", *Basin Research*, 1(3), 121-128, 1988.

4. Bulut, F., A. Doğru, C. Yaltirak, S. Yalvac and M. Elge, "Anatomy of October 30, 2020, Samos(Sisam)-Kuşadası Earthquake (MW 6.92) and Its Influence on Aegean Earthquake Hazard.", *Turkish Journal of Earth Sciences*, 30(4), 425-435, 2021.

5. Toda, S., R. S. Stein, V. Sevilgen and J. Lin, "Coulomb 3.3 Graphic-rich Deformation and Stress-change Software for Earthquake, Tectonic, and Volcano Research and Teaching User Guide.", *US Geological Survey Open-file Report, 1060(2011)*, 63, 2011.

6. Ellsworth, W. L. "Magnitude and Area Data for Strike Slip Earthquakes.", *US Geol. Surv. Open File Rep, 2003*, 03-214, 2003.

7. Okada, Y., "Surface Deformation due to Shear and Tensile Faults in a Half-space.", *Bulletin of the Seismological Society of America*, 75(4), 1135-1154, 2012.

8. Labuz, J. F. and A. Zang, "Mohr–Coulomb Failure Criterion.", *Rock Mechanics and Rock Engineering*, 45(6), 975-979, 2012.

9. Wells, D. L. and K. J. Coppersmith, "New Empirical Relationships Among Magnitude, Rupture Length, Rupture Width, Rupture Area, and Surface Displacement.", *Bulletin of the Seismological Society of America*, 84(4), 974-1002, 1994.

10. Reasenberg, P. A. and R. W. Simpson, “Response of Regional Seismicity to the Static Stress Change Produced by the Loma Prieta Earthquake.”, *Science*, 255(5052), 1687-1690, 1992.

11. Reid, H. F., “The California Earthquake of April 18, 1906”, *Report of the State Earthquake Investigation Commission*, Vol. 2, pp. 16–18, 1910.

12. Dogru, A., E. Gorgun, H. Ozener and B. Aktug, “Geodetic and Seismological Investigation of Crustal Deformation near Izmir (Western Anatolia).”, *Journal of Asian Earth Sciences*, 82, 21-31, 2014.

13. Al-Ajmi, A. M. and R. W. Zimmerman, “Relation between the Mogi and the Coulomb Failure Criteria.”, *International Journal of Rock Mechanics and Mining Sciences*, 42(3), 431-439, 2005.

14. Bulut, F., M. Bohnhoff, T. Eken, C. Janssen, T. Kılıç and G. Dresen, “The East Anatolian Fault Zone: Seismotectonic setting and spatiotemporal characteristics of seismicity based on precise earthquake locations.”, *Journal of Geophysical Research: Solid Earth*, 117(B7), 2012.

15. Hanks, T. C. and H. Kanamori, “A Moment Magnitude Scale.”, *Journal of Geophysical Research*, 84(B5), 2348-2350, 1979.

16. Reilinger, R., S. McClusky, P. Vernant, S. Lawrence, S. Ergintav, R. Cakmak, H. Ozener, F. Kadirov, I. Guliev, R. Stepanyan, M. Nadariya, G. Hahubia, S. Mahmoud, K. Sakr, A. ArRajehi, D. Paradissis, A. Al-Aydrus, M. Prilepin, T. Guseva, E. Evren, A. Dmitrotsa, S. V. Filikov, F. Gomez, R. Al-Ghazzi and G. Karam, “GPS Constraints on Continental Deformation in the Africa-Arabia-Eurasia Continental Collision Zone and Implications for the Dynamics of Plate Interactions.”, *Journal of Geophysical Research: Solid Earth*, Vol. 111, No. B5, 2006.

17. Yaltırak, C., E. B. İşler, A. E. Aksu and R. N. Hiscott, (2012). “Evolution of the Bababurnu Basin and Shelf of the Biga Peninsula: Western Extension of the Middle Strand of the North Anatolian Fault Zone, Northeast Aegean Sea, Turkey.”, *Journal of Asian Earth Sciences*, 57, 103-119, 2012.